

# Multiple Sensor Sequential Tracking of Neural Activity: Algorithm and FPGA Implementation

Lifeng Miao, Jun Jason Zhang, Chaitali Chakrabarti, Antonia Papandreou-Suppappola

School of Electrical, Computer and Energy Engineering, Arizona State University, Tempe, AZ  
E-mails: Lifeng.Miao@asu.edu, Jun.Zhang.EE@asu.edu, chaitali@asu.edu, papandreou@asu.edu

**Abstract**—We investigate the use of the particle filtering sequential Bayesian estimation technique and its hardware implementation for tracking neural activity. We propose using the multiple particle filter (MPF) approach in order to reduce the computational intensity incurred due to the large number of sensors required to observe the noninvasive magnetoencephalography (MEG) measurements needed to estimate the brain current dipole source locations and moments when tracking neural activity. The improved tracking performance of the MPF is demonstrated using numerical simulations on synthetic and real data. We also investigate the parallel implementation of the MPF algorithm on a Xilinx Virtex-5 field-programmable gate array (FPGA) platform. Our results of significant reduction in timing requirements demonstrate that the implementation is suitable for real-time tracking.

## I. INTRODUCTION

Localizing and tracking neural activity using noninvasive MEG measurements can provide very useful information during epilepsy surgery for patients with medically uncontrolled partial seizures [1]. Although MEG measurements provide high temporal resolutions in the order of milliseconds, it does not provide high spatial resolutions for neuronal activity localization. As a result, sensors are placed on the head at hundreds of locations in order to monitor brain magnetic fields [2], [3]. Since most MEG signals result from the intracellular longitudinal currents along active cortex regions, current dipoles have been successfully used to model brain activity [4], [5]. Following the multiple current dipole representation of electric sources, estimating dipole source characteristics using MEG measurements corresponds to determining the brain’s electrical current distributions [6]. Sequential Bayesian estimation techniques, such as particle filtering (PF) [7], have been used to track the dipole MEG source locations [8]. Note, however, that when tracking multiple neural activities, the number of dipole locations and moments increases. Consequently, the number of particles required for accurate tracking performance also increases, resulting in a significant increase in the PF computational complexity.

In this paper, we propose tracking neural activities using the multiple particle filter (MPF) approach [9] in order to reduce the PF computational complexity and improve the mean-squared error (MSE) estimation performance of the

multi-dipole localization problem. Using the MPF, the high-dimensional multi-dipole state model is divided into multiple, low-dimensional, single-dipole state models. We use separate, parallel, but interactive sub-PFs for tracking each dipole, resulting in largely-reduced particle numbers for each sub-PF and thus higher implementation efficiency. We implement the resulting algorithm on a Xilinx Virtex-5 FPGA platform to demonstrate its applicability to real-time MEG systems.

## II. MULTIPLE PARTICLE FILTERING

### A. Particle Filtering

Particle filtering (PF) is a sequential Monte Carlo method that can be used to estimate dynamic state parameters of nonlinear and/or non-Gaussian systems, by solving the (possibly) nonlinear state-space model, at time step  $k$ , given by

$$\mathbf{X}_k = f_k(\mathbf{X}_{k-1}, \mathbf{u}_{k-1}) \quad (1)$$

$$\mathbf{Z}_k = h_k(\mathbf{X}_k) + \mathbf{v}_k. \quad (2)$$

Here,  $\mathbf{X}_k$  is the state parameter vector of dimension  $n_x$ ,  $\mathbf{Z}_k$  is the measurement vector of dimension  $n_z$ ,  $f_k$  is the state-transition function,  $h_k$  is function that relates the state vector with the measurement vector,  $\mathbf{u}_k$  is the state modeling error process and  $\mathbf{v}_k$  is the measurement noise process. The PF approximates the state posterior probability density function (PDF) of  $\mathbf{X}_k$ , at time  $k$ , using a set of  $N$  samples or particles,  $\mathbf{X}_k^i$ , and their corresponding weights,  $w_k^i$ ,  $i = 1, \dots, N$  as

$$p(\mathbf{X}_k | \mathbf{Z}_k) \approx \sum_{i=1}^N w_k^i \delta(\mathbf{X}_k - \mathbf{X}_k^i).$$

The PF algorithm has three main steps: (a) the particles  $\mathbf{X}_k^i$  are drawn from an importance density  $q(\mathbf{X}_k | \mathbf{X}_{k-1}^i, \mathbf{Z}_{1:k})$ , where  $\mathbf{Z}_{1:k} = \{\mathbf{Z}_1, \dots, \mathbf{Z}_k\}$  is the sequence of all measurements up to time  $k$ ; (b) the weights are calculated as

$$w_k^i \propto w_{k-1}^i p(\mathbf{Z}_k | \mathbf{X}_k^i) p(\mathbf{X}_k^i | \mathbf{X}_{k-1}^i) / q(\mathbf{X}_k^i | \mathbf{X}_{k-1}^i, \mathbf{Z}_{1:k})$$

and then normalized so that  $\sum_{i=1}^N w_k^i = 1$ ; and (c) the particles are resampled to avoid particle degeneracy [7]. These three steps are the basis of the most commonly used PF algorithm, called sample-importance-resampling (SIR) PF.

## B. Multiple Particle Filtering

If the dimension  $n_x$  of the state vector  $\mathbf{X}_k$  is large, a large number of particles would be required to accurately estimate the state. For  $n_x > 1$ , the state vector can be represented by  $\mathbf{X}_k = [\mathbf{X}_{k,1}^\top \mathbf{X}_{k,2}^\top \dots \mathbf{X}_{k,J}^\top]^\top$ , where  $\top$  denotes vector transpose and each subvector  $\mathbf{X}_{k,j}$  is of dimension  $L = n_x/J$  (with  $L$  assumed to be an integer). The state update equation for the  $j$ th sub-vector,  $j = 1, 2, \dots, J$ , is given by

$$\mathbf{X}_{k+1,j} = f(\mathbf{X}_{k,j}, \mathbf{u}_{k,j}),$$

where  $\mathbf{u}_{k,j}$  is the  $j$ th modeling error process of dimension  $L$ .

A different PF needs to be used for each sub-vector  $\mathbf{X}_{k,j}$ , using  $N_j$  particles  $\mathbf{x}_{k,j}^{(i)}$  with corresponding weights  $w_{k,j}^{(i)}$ ,  $i = 1, \dots, N_j$  and  $j = 1, \dots, J$ . When implementing the MPF, the particle propagation and resampling steps are the same as with the SIR PF. However, the weight updating step is different and given by [9]

$$w_{k,j}^{(i)} \propto w_{k-1,j}^{(i)} \frac{p(\mathbf{z}_k | \mathbf{x}_{k,j}^{(i)}, \tilde{\mathbf{x}}_{k,-j}) p(\mathbf{x}_{k,j}^{(i)} | \mathbf{x}_{k-1,j}^{(i)}, \hat{\mathbf{x}}_{k-1,-j})}{q_j(\mathbf{x}_{k,j}^{(i)} | \mathbf{x}_{k-1,j}^{(i)}, \tilde{\mathbf{x}}_{k-1,-j}, \mathbf{z}_k)}$$

where  $\tilde{\mathbf{x}}_{k,-j}$  and  $\hat{\mathbf{x}}_{k-1,-j}$  are predicted and estimated values of all the states at time step  $k$  except of the  $j$ th state vector  $\mathbf{x}_{k,j}$ , respectively. If the same importance density is used by all sub-vectors, that is,  $q_j(\mathbf{x}_{k,j} | \mathbf{x}_{k-1,j}, \mathbf{z}_k) = p(\mathbf{x}_{k,j} | \mathbf{x}_{k-1,j})$ , then the weight update function is reduced to

$$w_{k,j}^{(i)} \propto w_{k-1,j}^{(i)} p(\mathbf{z}_k | \mathbf{x}_{k,j}^{(i)}, \tilde{\mathbf{x}}_{k,-j}), \quad (3)$$

where the predicted values are obtained from

$$\tilde{\mathbf{x}}_{k,j} = \sum_{i=1}^{N_j} w_{k,j}^{(i)} \mathbf{x}_{k,j}^{(i)}. \quad (4)$$

The sub-vector state-space formulation suggests that, at each time step  $k$ , the  $j$ th PF obtains a prediction of its state and provides the information to the remaining  $J-1$  PFs. The PFs use the exchanged information for computing the weights of their particles and eventually for generating new particles.

## III. MPF FOR LOCALIZING NEURAL ACTIVITY

### A. MEG Inverse Problem

According to the quasi-static approximation in [10], a current density  $I_k(\mathbf{p})$  at location  $\mathbf{p}$  and time instant  $k$  inside a volume  $\Omega$  produces the magnetic field  $b_k(\mathbf{p}_s)$  due to a sensor at location  $\mathbf{p}_s$ . According to the Biot-Savart equation, this magnetic field is given by

$$b_k(\mathbf{p}_s) = \frac{\mu_0}{4\pi} \int_{\Omega} I_k(\mathbf{p}) \times \frac{\mathbf{p}_s - \mathbf{p}}{|\mathbf{p}_s - \mathbf{p}|^3} d\mathbf{p}, \quad (5)$$

where  $\mu_0$  is the constant magnetic permittivity of vacuum in volume  $\Omega$ . When considering the magnetic field generated from the human brain, the current density consists of two terms: the *primary current*  $I_k^{(pc)}(\mathbf{p})$  of neural origin, and the *volume current*  $I_k^{(v)}(\mathbf{p})$  that is due to the nonzero conductivity of the human brain. The MEG inverse problem is thus the recovery of  $I_k^{(pc)}(\mathbf{p})$  from the measured magnetic field produced by both current densities.

The magnetic field in (5) can be simplified based on some assumptions. The first assumption is that the *primary current* can be represented by one or multiple ideal point-like *current dipoles* as [4]

$$I_k^{(pc)}(\mathbf{p}) = \sum_{j=1}^{N_d} \mathbf{m}_{k,j} \delta(\mathbf{p} - \mathbf{p}_{k,j}),$$

where  $\mathbf{p}_{k,j} = [p_{k,j}^{(x)} p_{k,j}^{(y)} p_{k,j}^{(z)}]^\top$  and  $\mathbf{m}_{k,j} = [m_{k,j}^{(x)} m_{k,j}^{(y)} m_{k,j}^{(z)}]^\top$  are the three-dimensional (3-D) location and moment vectors, respectively, in Cartesian coordinates, of the  $j$ th current dipole. The  $j$ th current dipole can thus be represented by the 6-D state vector  $\mathbf{X}_{k,j} = [\mathbf{p}_{k,j}^\top \mathbf{m}_{k,j}^\top]^\top$ . The second assumption is that the model for the human head can be simplified to a sphere of constant conductivity  $\sigma$ , whose explicit value is not actually needed for neural tracking.

Given these two assumptions, an analytic formula which accounts for the contributions of both the primary and volume currents is given by [10]

$$b_k(\mathbf{p}_s) = \sum_{j=1}^{N_d} \frac{\mu_0}{4\pi g_{k,j}^2} (g_{k,j} \mathbf{m}_{k,j} \times \mathbf{p}_{k,j} - (\mathbf{m}_{k,j} \times \mathbf{p}_{k,j} \cdot \mathbf{p}_s) \nabla g_{k,j}), \quad (6)$$

where  $g_{k,j} = a_{k,j}(p_s a_{k,j} + p_s^2 - (\mathbf{p}_{k,j} \cdot \mathbf{p}_s))$ ,  $a_{k,j} = |\mathbf{p}_s - \mathbf{p}_{k,j}|$ ,  $p_s = |\mathbf{p}_s|$  and  $\nabla g_{k,j}$  is defined in [10]. Also, if  $\mathbf{a} = [a_1 a_2 a_3]^\top$  and  $\mathbf{b} = [b_1 b_2 b_3]^\top$ , then their cross product is given by  $\mathbf{a} \times \mathbf{b} = [a_1 b_2 - a_2 b_1, a_2 b_3 - a_3 b_2, a_3 b_1 - a_1 b_3]^\top$  and their dot product is  $\mathbf{a} \cdot \mathbf{b} = a_1 b_1 + a_2 b_2 + a_3 b_3$ . The inverse problem dynamically estimates the 3-D location  $\mathbf{p}_{k,j}$  and 3-D moment  $\mathbf{m}_{k,j}$  from the magnetic measurements  $b_k(\mathbf{p}_s)$ . From Equation (6), we can see that the problem is nonlinear though the dependence of  $b_k(\mathbf{p}_s)$  on the dipole moments  $\mathbf{m}_{k,j}$  is linear. As a result, the PF can be used to estimate the location  $\mathbf{p}_{k,j}$  and moment  $\mathbf{m}_{k,j}$  vectors, and Equation (6) can be used as the measurement equation.

### B. Tracking Neural Activity Using MPF

We first model the brain as a 3-D sphere and consider the single dipole tracking problem [6]. The magnetometers are distributed on a spherical hemisphere of radius  $r_{\text{obs}} > 0$  with radial orientation. The radius of the sphere model of the brain is  $r_{\text{max}} < r_{\text{obs}}$ . We ignore the volume currents and also assume that the activity is confined to the volume  $V$  in the upper half space  $z > 0$  such that the radial distance  $r$  from the origin satisfies  $r_{\text{min}} < r < r_{\text{max}}$ . Using Cartesian coordinates, the 3-D dipole position is  $\mathbf{p}_{k,1} = [p_{k,1}^{(x)} p_{k,1}^{(y)} p_{k,1}^{(z)}]^\top$  and the 3-D dipole moment is  $\mathbf{m}_{k,1} = [m_{k,1}^{(x)} m_{k,1}^{(y)} m_{k,1}^{(z)}]^\top$ . The unknown state at time  $k$  is thus denoted by the 6-D state vector  $\mathbf{X}_k = [\mathbf{p}_{k,1}^\top \mathbf{m}_{k,1}^\top]^\top$ .

The single dipole state-space model for the MEG source localization problem is given by [8]:

$$\mathbf{X}_{k+1} = \mathbf{X}_k + \mathbf{u}_k, \quad \mathbf{Z}_k = h(\mathbf{X}_k) + \mathbf{v}_k, \quad (7)$$

where the  $\Gamma$ -dimensional vector  $\mathbf{Z}_k$  is the MEG sensor measurement at time  $k$ ,  $\Gamma$  is the number of magnetometers,  $\mathbf{u}_k$  and  $\mathbf{v}_k$  are the process noise and measurement noise,

respectively, and  $h(\cdot)$  is a nonlinear gain function that depends on the relation between the brain's external magnetic field and internal current density. Specifically,  $\mathbf{Z}_k = [b_{k,1} \dots b_{k,\Gamma}]^\top$ , where

$$b_{k,\gamma} = \frac{\mu_0}{4\pi} \frac{\mathbf{m}_{k,1} \times (\mathbf{p}_{k,\gamma} - \mathbf{p}_{k,1})}{|\mathbf{p}_{k,\gamma} - \mathbf{p}_{k,1}|^3}, \quad \gamma = 1, \dots, \Gamma, \quad (8)$$

where  $\mathbf{m}_{k,1}$  and  $\mathbf{p}_{k,1}$  are the moment and location of the single dipole, and  $\mathbf{p}_{k,\gamma}$  is the location of the  $\gamma$ th sensor. In practice, however, we do not necessarily have only one well-localized active region. We thus extend the particle filtering approach to the case of  $N_d$  dipoles.

For the multiple dipole formulation, the unknown state has dimension  $6N_d$  and the  $\Gamma$ -dimensional magnetic field measurements  $\mathbf{Z}_k = [b_{k,1} \dots b_{k,\Gamma}]^\top$  are given by

$$b_{k,\gamma} = \frac{\mu_0}{4\pi} \sum_{j=1}^{N_d} \frac{\mathbf{m}_{k,j} \times (\mathbf{p}_{k,\gamma} - \mathbf{p}_{k,j})}{|\mathbf{p}_{k,\gamma} - \mathbf{p}_{k,j}|^3}, \quad \gamma = 1, \dots, \Gamma. \quad (9)$$

For the MPF formulation, we divide the  $6N_d$ -dimensional multi-dipole state vector  $\mathbf{X}_k$  into  $N_d$  single-dipole state 6-D vectors  $\mathbf{X}_{k,j} = [p_{k,j}^{(x)} p_{k,j}^{(y)} p_{k,j}^{(z)} m_{k,j}^{(x)} m_{k,j}^{(y)} m_{k,j}^{(z)}]^\top$ ,  $j=1, \dots, N_d$ . In order to still improve computational complexity for the case of the single dipole, we divide the 6-D state vector  $\mathbf{X}_k$  into two 3-D sub-vectors,  $\mathbf{X}_{k,1} = [p_{k,1}^{(x)} p_{k,1}^{(y)} p_{k,1}^{(z)}]$  and  $\mathbf{X}_{k,2} = [m_{k,1}^{(x)} m_{k,1}^{(y)} m_{k,1}^{(z)}]$ .

For  $N_d > 1$ , the  $j$ th sub-state space represents the location and moment of the  $j$ th dipole source,  $j = 1, \dots, N_d$ . It uses the  $j$ th PF to track the  $j$ th MEG source of neural activity. The particle generation and resampling step of each PF are implemented using the SIR approach [7]. However, the weight update step is modified to [9]

$$\mathbf{w}_{k,j}^{(i)} \propto \mathbf{w}_{k-1}^{(i)} p(\mathbf{Z}_k | \mathbf{X}_{k,j}^{(i)}, \tilde{\mathbf{X}}_{k,-j}), \quad i = 1, \dots, M_j$$

where  $M_j$  is the number of particles in the  $j$ th PF, and  $\tilde{\mathbf{X}}_{k,-j} = [\tilde{\mathbf{X}}_{k,1}^\top \dots \tilde{\mathbf{X}}_{k,j-1}^\top \tilde{\mathbf{X}}_{k,j+1}^\top \dots \tilde{\mathbf{X}}_{k,N}^\top]^\top$  and  $\hat{\mathbf{X}}_{k,-j} = [\hat{\mathbf{X}}_{k,1}^\top \dots \hat{\mathbf{X}}_{k,j-1}^\top \hat{\mathbf{X}}_{k,j+1}^\top \dots \hat{\mathbf{X}}_{k,N}^\top]^\top$  are the predicted and estimated values of all the states, excluding  $\tilde{\mathbf{X}}_{k,j}$  and  $\hat{\mathbf{X}}_{k,j}$ , respectively. Thus, the predicted values in Equation (7) are obtained as  $\tilde{\mathbf{X}}_{k,j} = \sum_{i=1}^{M_j} \mathbf{w}_{k-1,j}^{(i)} \mathbf{X}_{k,j}^{(i)}$ . Since we use a predicted value  $\tilde{\mathbf{X}}_{k,-j}$  instead of a set of random particles  $\mathbf{X}_{k,-j}^{(i)}$  to calculate the likelihood function  $p(\mathbf{Z}_k | \mathbf{X}_k^{(i)}) = p(\mathbf{Z}_k | \mathbf{X}_{k,j}^{(i)}, \tilde{\mathbf{X}}_{k,-j})$ , the number of particles needed can be significantly reduced.

#### IV. NEURAL ACTIVITY TRACKING RESULTS

##### A. Synthetic Data Results

The MSE performance results are first demonstrated with the proposed MPF approach for both the single-dipole and the multiple-dipole neural activity tracking problem using synthetic data. The data was created by inserting current dipoles into the sphere head model and calculating the resulting magnetic field using Equation (9) with Gaussian noise. Figures 1(a) and 1(b) compares the true location and moment of the  $x$  Cartesian coordinate of the dipole with the estimated ones obtained using both the SIR PF (SPF) tracker and the

MPF tracker. Note that the SPF used 5,000 particles, and each of the two sub-PFs of the MPF used 1,000 particles each. For the  $N_d=2$  multi-dipole case, the tracking results are shown in Figures 1(c)-1(f). The MPF used two SPFs with 5,000 particles each, and the PF used 20,000 particles.

The average MSE comparison for 100 Monte Carlo simulations for both dipole cases is summarized in Tables I and II. Although both trackers provide reasonable estimates of the MEG source locations, the MPF tracker needs significantly fewer number of particles. When the MPF tracker uses the same number of particles as the SPF, then the MPF results in improved MSE performance. For example, the MSE performance improves from 0.398 to 0.253 for the single-dipole model and from 0.576 to 0.377 for the two-dipole model.

TABLE I  
COMPARISON OF MSE FOR SINGLE-DIPOLE MODEL

Approach	SPF	Multiple PF	
Number of particles	5,000	2,000	5,000
3-D Location MSE	0.398	0.363	0.253
3-D Moment MSE	0.332	0.295	0.206

TABLE II  
COMPARISON OF MSE FOR TWO-DIPOLE MODEL

Approach	SPF	Multiple PF	
Number of particles	20,000	10,000	20,000
Dipole1 Location MSE	0.576	0.491	0.377
Dipole2 Location MSE	0.547	0.486	0.359

##### B. Real Data Results

The performance the new MPF approach is also compared with the SPF using real data from a language study experiment [11]. In this experiment, 87 incongruent sentences were given to the subjects sequentially. After a 300 ms warning tone, followed by a 1,200 ms pause, a sentence was presented. The time lapse between two sentences was 4,100 ms. MEG signals were recorded with a 151 sensor CTF Omega System, lowpass filtered at 100 Hz, and digitized at 300 Hz. The MEG data was averaged from 87 trials to increase the signal-to-noise ratio (SNR). The tracking trajectory results are shown in Figure 2. Figure 3 compares the tracking performance of the SPF and the MPF with a dipole fitting beamformer technique that uses a spatially adaptive filter to estimate the amount of activity at any given location in the brain [11], [12]. For the particle filtering techniques, we used 10,000 particles for the SPF and 5,000 particles for each of the sub-PFs of the MPF. Note that for the real data, we do not have the accurate location of the source dipoles, so cannot say if our method is working better than the beamformer dipole fitting method.

#### V. HARDWARE IMPLEMENTATION

##### A. Architecture Overview

The overall block diagram of the proposed hardware architecture is shown in Fig. 4(a). It consists of  $J=N_d$  processing elements (PE) connected by a global bus, where  $N_d$  is the number of current dipoles and also the number of sub-PFs. Each PE implements the computation steps for one sub-PF

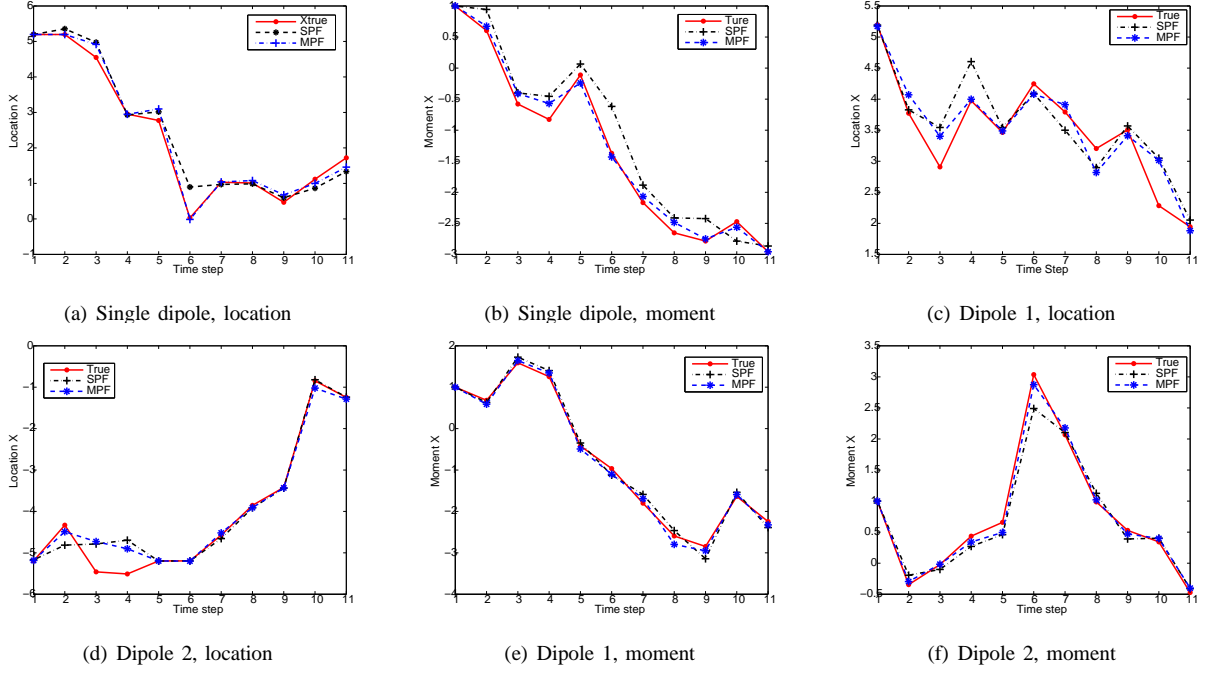


Fig. 1. Comparison between the true (red) and estimated, using SIR PF or SPF (black) and MPF (blue),  $x$  Cartesian coordinate of (a) single dipole location; (b) single dipole moment; (c) Dipole 1 location; (d) Dipole 2 location; (e) Dipole 1 moment; and (f) Dipole 2 moment.

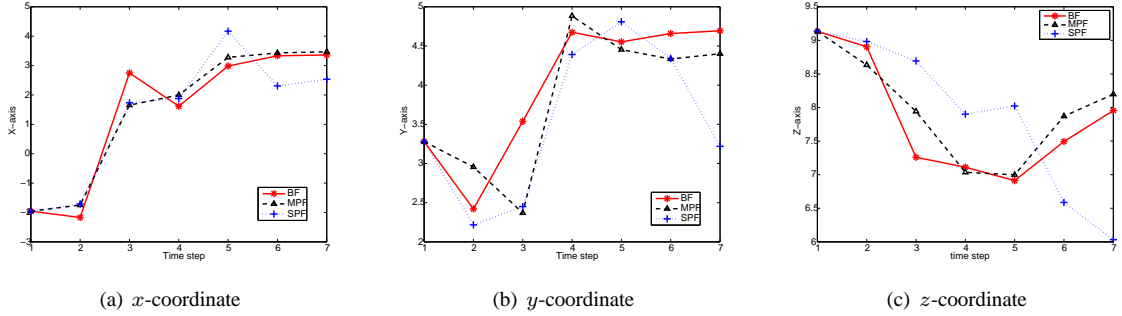


Fig. 3. Tracking performance for estimating the dipole location using real data using beamformer method (BF), SIR PF (SPF), and MPF.

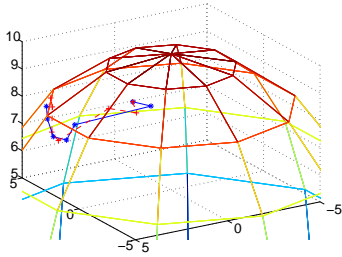


Fig. 2. 3-D location coordinate tracking result using real data.

concurrently as shown in Fig. 4(a). The inter-PE communication is quite small: PE $_j$  transmits the predicted value  $\tilde{\mathbf{x}}_{j,k}$  to other PEs and receives  $\tilde{\mathbf{x}}_{-j,k}$  from other PEs to update the weights, where  $\tilde{\mathbf{x}}_{j,k}$  can be calculated using (4).

Here, we employ the parallel PF independent Metropolis-Hastings (PPF-IMH) architecture [13] which can significantly

reduce processing time and communication overhead. The block diagram of each PE is given in Figure 4(b). Each PE consists of four computing engines (CE) which operate in parallel and one central unit (CU). The  $M$  particles are equally distributed among four CEs, and the local PF processing steps, such as particle generation, weight evaluation and IMH resampling, are executed in each CE.

In order to reduce the communication overhead, the particles in each CE are distributed into groups based on the global range  $XL$  and  $XH$  computed in the CU. The average value  $\mu\tilde{\mathbf{x}}$  and average weight  $\mu w$  of the particles in the group are used to form the new particles. This method may affect the estimation accuracy since the average value in each group is replicated. To improve estimation performance while keeping the communication overhead low, we use IMH resampling in each CE and transmit the range of the resampled particles to the CU. The resampled particles represent the posterior proba-

bility density function more accurately, thereby improving the estimation performance. In addition, since the IMH sampler can be easily pipelined, the processing period is not increased.

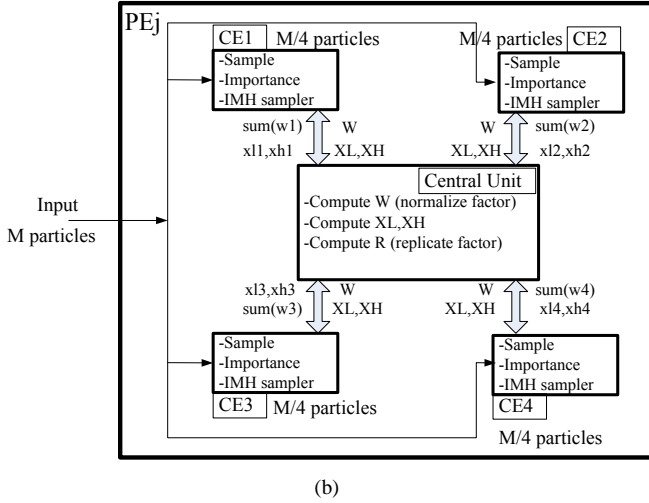
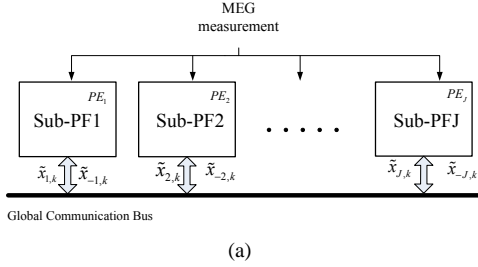


Fig. 4. Block diagram: (a) overall architecture; (b) PPF-IMH architecture.

### B. Hardware Implementation Evaluation

The MPF PPF-IMH hardware architecture is implemented using Verilog HDL and synthesized on the Xilinx Virtex-5 device (XC5VSX240T). The design was verified using Modelsim.

**Resource Utilization:** Table III summarizes the architecture resource utilization for a two-dipole, 8,000 particle system. Each dipole is processed by a sub-PF, each sub-PF consists of 4 CEs, and each CE processes 1,000 particles. The exponential functions are implemented using CORDIC units, and the rest of the units are implemented using DSP cores.

TABLE III  
RESOURCE UTILIZATION ON XILINX XC5VSX240T

Unit	Occupied slices	Slice Reg.	Slice LUTs	Block Ram	DSP48Es
4-CE	25,820 (68%)	81,837 (54%)	84,164 (56%)	247 (47%)	606 (57%)

**Execution Time:** Figure 5 shows the timing for one iteration of the proposed method. For our implementation,  $M/4=1000$ ,  $L_s=2$  is the sampling step delay,  $L_w=78$  is the weighting latency determined by the calculation period of the exponential functions,  $L_r=12$  is the latency of calculating the global ranges, and  $L_\rho=23$  is the computing time for the replication factor. Thus, one iteration takes  $T_{total}=(L_s + M/4 + L_w + M/4 + L_r + M/4 + L_\rho) \times T_{clk}=3,115$  cycles. We choose the

system clock rate as 100 MHz. The total processing period for one iteration is only  $T_{total}=31.15 \mu s$ .

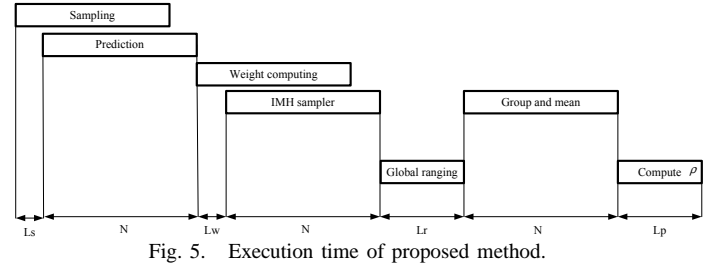


Fig. 5. Execution time of proposed method.

## VI. CONCLUSION

In this paper, we proposed the application of multiple particle filtering for tracking neural activity and demonstrated its performance using both synthetic and real data. This method achieves better tracking performance in terms of MSE using the same number of particles as the SIR PF. When using lower lower number of particles for each sub-PF than the SIR PF, it achieves the same MSE but with a highly reduced computational complexity. The proposed method was also implemented on the Xilinx Virtex-5 FPGA platform. The processing time for one iteration using 8,000 particles was shown to be only 31.15  $\mu s$ .

## REFERENCES

- [1] D. Cohen, "Magnetoencephalography: Evidence of magnetic fields produced by alpha rhythm currents," *Science*, vol. 161, pp. 664–666, June 1972.
- [2] F. Darvas, D. Pantazis, E. Kucukaltun-Yildirim, and R. M. Leahy, "Mapping human brain function with MEG and EEG: Methods and validation," *Mathematics in Brain Imaging*, vol. 23, pp. 289–299, 2004.
- [3] S. Baillet, J. C. Mosher, and R. M. Leahy, "Electromagnetic brain mapping," *IEEE Signal Processing Magazine*, vol. 18, pp. 14–30, 2001.
- [4] K. Uutela, M. Hämäläinen, and R. Salmelin, "Global optimization in the localization of neuromagnetic sources," *IEEE Transactions on Biomedical Engineering*, vol. 45, pp. 716–723, 1998.
- [5] K. Jerbi, J. C. Mosher, S. Baillet, and R. M. Leahy, "On MEG forward modelling using multipolar expansions," *Physics in Medicine and Biology*, vol. 47, no. 4, pp. 523–555, 2002.
- [6] M. Hämäläinen, R. Hari, R. J. Ilmoniemi, J. Knuutila, and O. V. Lounasmaa, "Magnetoencephalography—theory, instrumentation and applications to noninvasive studies of the working human brain," *Reviews of Modern Physics*, vol. 65, pp. 413–497, 1993.
- [7] M.S. Arulampalam, S. Maskell, N. Gordon, and T. Clapp, "A tutorial on particle filters for online nonlinear/non-Gaussian Bayesian tracking," *IEEE Transactions On Signal Processing*, vol. 50, pp. 174–188, 2002.
- [8] E. Somersalo, A. Voutilainen, and J. P. Kaipio, "Non-stationary magnetoencephalography by Bayesian filtering of dipole models," *Inverse Problems*, vol. 19, pp. 1047–1063, 2004.
- [9] P. M. Djuric, T. Lu, and M. F. Bugallo, "Multiple particle filtering," in *IEEE International Conference on Acoustics, Speech, and Signal Processing*, June 2007, pp. 1181–1184.
- [10] J. Sarvas, "Basic mathematical and electromagnetic concepts of the biomagnetic inverse problem," *Physics in Medicine and Biology*, vol. 32, pp. 11–12, 1987.
- [11] "FieldTrip Matlab software toolbox for MEG and EEG analysis," <http://fieldtrip.fcdonders.nl>.
- [12] J. Gross, J. Kujala, M. Hamalainen, L. Timmermann, A. Schnitzler, and R. Salmelin, "Dynamic imaging of coherent sources: Studying neural interactions in the human brain," *Proc. of the National Academy of Sciences*, vol. 98, pp. 694–699, January 2001.
- [13] L. Miao, J. J. Zhang, C. Chakrabarti, and A. Papandreou-Suppappola, "A new parallel implementation for particle filters and its application to adaptive waveform design," *IEEE Workshop on Signal Processing Systems*, pp. 19–24, October, 2010.